Journal of Hydraulic Structures
J. Hydraul. Struct., 2022; 7(3):56-71
DOI: 10.22055/JHS.2022.41941.1233

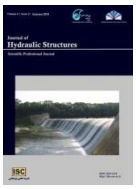

OPEN ACCESS

Sensitivity Analysis of Weakly Compressible Moving Particle Semi-Implicit Method in a Dam-Break Flow Simulation

Sadegh Moodi [1]
Mehdi Azhdary Moghaddam [2]
Hossein Mahdizadeh [3]

Abstract

Lagrangian approaches such as the Moving Particle Semi-Implicit method and Smoothed particle Hydrodynamics are the latest techniques in Computational Fluids Dynamics and have attracted the attention of many researchers. Due to the Lagrangian nature of such practices, they can simulate various problems with large deformations and a variety of boundary conditions which has led to their application in many complex engineering problems. Therefore, the accuracy of the results obtained using these methods is substantial, while various parameters affect the accuracy of the simulation. In this paper, the sensitivity of a dam-break flow simulated by the Weakly Compressible Moving Particle Semi-Implicit method associated with the particle size and Courant number is analyzed. The analysis is performed in two circumstances. First, the Courant number is fixed, and sensitivity relative to the particle size is investigated. Then, sensitivity relative to the Courant number is studied in fixed particle size. In general, it can be concluded that the smaller the particle size and Courant number, the higher accuracy and computational cost.

Keywords: Dam-Break Problem, Lagrangian Methods, Sensitivity Analysis, Weakly Compressible Moving Particle Semi-Implicit Method.

Received: 23 September 2022; Accepted: 30 November 2022

1. Introduction

Dam break flows propagate through the length of rivers and flood zones, leading to intense damage and flooding; Accordingly, many experimental, analytical, and numerical studies have been performed considering the dam break problem as an important issue [1-4]. The modeling of flow structure becomes more complex with a violent flow. Numerical simulation of free-surface flows such as dam break problems has been according to Eulerian mesh-based methods such as FEM or FVM for several years[3-7]. Some studies have investigated dam break concerning the

[1] Department of Civil Engineering, University of Sistan and Baluchestan, Zahedan, Iran.
[2] Department of Civil Engineering, University of Sistan and Baluchestan, Zahedan, Iran. E-mail: mazhdary@eng.usb.ac.ir **(Corresponding Author).**
[3] Department of Civil Engineering, University of Birjand, Birjand, Iran.

CC BY

free surface, velocity, pressure, and the movement of the wavefront [8-11]. For example, Ritter [12] provided an analytical solution for dam-break flow based upon the inviscid fluids equation of Saint-Venant on a smooth, dry surface in the horizontal direction. Deng et. al [13] proposed a method using a relation between time and the velocity of the wave to solve 2D shallow water equations. Ozmen-Catagay and Kocaman [14] performed a numerical and experimental study of the dam break flow on a dry bed. They simulated the flow employing Reynolds Averaged Navier-Stokes (RANS) equations and shallow water equations (SWEs) and compared them with experimental measurements and generally found that the RANS equations could better model free-surface profiles but suffered from a more computational time.

When the mesh-based approaches encounter large deformations of a free surface or an interface, some problems have arisen. Some numerical methods have been proposed to enable the Eulerian techniques to simulate deformations and fragmentations of free surfaces [15, 16]. Nonetheless, the maintenance of sharp or fragmented interfaces and treating the cells containing free surfaces, are the principal difficulties in implementing such methods [17]. In addition, the issue of numerical dispersion because of advection components is prevalent in these approaches [18, 19]. Developing a new generation of numerical techniques has been the focus of CFD researchers. Lagrangian methods have a practical advantage in encountering large deformations and fragmentation of interfaces compared to traditional grid-based approaches [20]. Particle methods consider a set of separate particles in a Lagrangian framework [20].

There are many types of meshless methods and they have a wide range of applications [21, 22]. One of the widely-used particle approaches is the Smoothed Particle Hydrodynamics (SPH) method [23-26] has been applied in various areas, such as dam-break flows [27-30]. Koshizuka and Oka [31] proposed the Moving Particle Semi-Implicit (MPS) method close to the SPH approach, although it takes advantage of a weight-averaging operation. The ability of these methods to simulate the dam break flow on a wet and dry surface has been shown so far [32-34]. In addition, the MPS method application in some other free surface issues such as wave breakers [18, 19], flow on spillways [35], and hydraulic jumps [33] has been successful. This mesh-free method was then improved with various techniques such as extended spatial models [36, 37], dynamic stabilization technique [38], and particle displacement [39], which enabled this method to deal with engineering problems.

The original version of the MPS method implicitly solves the Poisson equation to calculate the pressure. Shakibaeinia et. al [33] proposed the Weakly Compressible Moving Particle Semi-Implicit Method (WC-MPS) to solve the problem of artificial pressure fluctuation in the preliminary version of this method. Fu et. al [40] utilized this method to simulate dam-break flow and validate this method using velocity and free surface distribution. The validation of the WC-MPS method to create the profiles of free surface and efficient pressure was the subject of the other studies [37, 41]. Shakibaeinia and Jin modeled a dam-break flow on a moving bed, developing a new version of the WC-MPS method [42].

Accuracy is one of the most critical factors in approving a method. It is always necessary to control the factors that overshadow this accuracy and determine the effect of each. Therefore, sensitivity analysis can be used to evaluate and increase the accuracy of methods. Previous studies have not analyzed the sensitivity of the WC-MPS method. Therefore, the purpose of the present study is to examine the sensitivity of this method to the particle size and the Courant number in simulating a dam-break flow.

2. Material and methods

2.1. MPS Method

Particles in the MPS method move based on equations determining the laws of the phenomena. The governing equations of this method are the Navier-Stokes equations and the continuity equation, which are the governing regulation of a fluid, i.e., conservation of momentum and mass conservation. The Navier-Stokes equation is [33]:

$$\frac{D\boldsymbol{u}}{Dt} = -\frac{1}{\rho}\nabla P + \upsilon\nabla^2\boldsymbol{u} + \boldsymbol{g} \tag{1}$$

In which the velocity vector is represented by u. P, ρ, and υ are the pressure, fluid density, and kinematic viscosity, respectively. In addition, ∇P is the pressure gradient, $\upsilon\nabla^2\boldsymbol{u}$ represents the viscosity term, g is the external force term, and t shows the time.
The continuity equation is [33]:

$$\frac{D\rho}{Dt} + \rho\nabla.\boldsymbol{u} = 0 \tag{2}$$

The continuity equation states mass conservation. The computational domain in the MPS approach is represented by a finite number of particles in space moving freely. A particle can also be affected by neighboring particles. Based on the definition of the MPS method, this interaction occurs when the neighboring particles are located in the radius of r_e of the particle, which in this paper equals r_e=3.2δL, with δL the mean particle size.

The interaction of particles in the MPS methods is calculated by choosing a kernel function. In this paper, a third-order spiky polynomial function is utilized for high-resolution simulation [33].

$$W(r_{ij}, r_e) = \begin{cases} \left(1 - \frac{r_{ij}}{r_e}\right)^3 & 0 \le \left(\frac{r_{ij}}{r_e}\right) < 1 \\ 0 & \left(\frac{r_{ij}}{r_e}\right) \ge 1 \end{cases} \tag{3}$$

r_e is the effective radius, and the absolute distance between particle i and the neighboring particle j is represented by r_{ij}. The particle number density is a dimensionless parameter and is used in the density measurement. It is calculated as [33]:

$$\langle n\rangle_i = \sum_{j\neq i} W(r_{ij}, r_e) \tag{4}$$

The application of the < > operator is the smoothed calculation of a quantity and can be written for f as:

$$\langle f\rangle_i = \frac{1}{n_0}\sum_{j\neq i} f_j W(r_{ij}, r_e) \tag{5}$$

n_0 is the mean initial particle number density. The approximation of the spatial derivatives can be performed using a similar approach. The gradient of a scalar *f* is given by:

$$\langle \nabla f \rangle_i = \frac{D}{n_0} \sum_{j \neq i} \frac{f_j - f_i}{r_{ij}} \boldsymbol{e}_{ij} W(r_{ij}, r_e) \tag{6}$$

where D represents the number of dimensions, and the unit vector of direction is defined as $\mathbf{e}_{ij} = \mathbf{r}_{ij}/r_{ij}$. The divergence and Laplacian of vector **F** are written as:

$$\langle \nabla \boldsymbol{F} \rangle_i = \frac{D}{n_0} \sum_{j \neq i} \frac{\boldsymbol{F}_j - \boldsymbol{F}_i}{r_{ij}} \boldsymbol{e}_{ij} W(r_{ij}, r_e) \tag{7}$$

$$\langle \nabla^2 \boldsymbol{F} \rangle_i = \frac{2D}{\lambda n_0} \sum_{j \neq i} \left((\boldsymbol{F}_j - \boldsymbol{F}_i) W(r_{ij}, r_e) \right) \tag{8}$$

In which λ is the representation of a correction parameter as [31]:

$$\lambda = \frac{\int_V W(r, r_e) r^2 dv}{\int_V W(r, r_e) dv} \approx \frac{\sum_{i \neq j} W(r_{ij}, r_e) r_{ij}^2}{\sum_{i \neq j} W(r_{ij}, r_e)} = \langle r_{ij}^2 \rangle \tag{9}$$

The momentum equation is then written in the following discretized form:

$$\left\langle \frac{D\boldsymbol{u}}{Dt} \right\rangle = -\frac{D}{\rho_i n_0} \sum_{i \neq j} \left(\frac{p_j - \hat{p}_i}{r_{ij}} \boldsymbol{e}_{ij} W(r_{ij}, r_e) \right) + \frac{2D}{\rho_i \lambda n_0} \sum_{i \neq j} \left(\frac{2 v_i v_j}{v_i + v_j} (\boldsymbol{u}_j - \boldsymbol{u}_i) W(r_{ij}, r_e) \right) + \boldsymbol{g} \tag{10}$$

$$\hat{p}_i = min(p_i, p_j); j \in \{ W(r_{ij}, r_e) \neq 0 \} \tag{11}$$

As mentioned above, particles in the MPS approach represent the mass. Therefore, mass conservation is satisfied automatically. A further equation is needed to approximate the pressure field. For this purpose, the fully incompressible MPS method utilizes Poisson's pressure equation. In the WC-MPS method, the equation of state is employed to measure the pressure field explicitly [33]:

$$p_i = \frac{c_0^2 \rho_0}{\gamma} \left(\left(\frac{n_i}{n_0} \right)^{\gamma} - 1 \right) \tag{12}$$

In which c_0 is the numerical sound speed, and ρ_0 represents the reference density. In addition, the value of γ is deemed to be 0.7. The sound speed is considered ten times or more the maximum velocity of the fluid to prevent instability and small values of time steps [43].

The Courant-Friedrichs-Lewy stability (CFL) condition has to be satisfied because an explicit time-splitting approach is utilized. The CFL condition is written as [44]:

$$\frac{|\boldsymbol{u}|_{max}}{\delta L} \delta t < C \tag{13}$$

In which $|\mathbf{u}|_{max}$ and δL are the maximum value of the velocity and the average distance between particles, respectively. δt represents the time interval, and C is the Courant number that should be in the range of (0,1].

2.2. Boundary conditions

In general, to define the problem, assigning boundary conditions is one of the essential issues. This subject is more critical in CFD because the efficiency of numerical methods and the quality of the results are directly related to the numerical treatment of boundary conditions. In the simulation by MPS, four types of boundary conditions can be used, including the solid wall, free surface, inlet/outlet boundary, and periodic boundary. In this research, solid walls and free surfaces have been used, which play a significant role in many problems. The representation of a solid wall would be a surface of solid objects which doesn't allow the fluid to pass through. The free surface is an interface that can deform between two separate phases of fluid, which are in two common types, gas and liquid. The vacuum assumption is usually used for the gas phase, resulting in a significant presence of gas. This idea helps to reduce the complexity of the problem considerably.

Here, a free surface dam-break flow is investigated for sensitivity analysis concerning particle size and Courant number. The definition of a free surface is the fluid being exposed to atmospheric pressure, which equals zero. The free surface in WC-MPS determines by:

$$\langle n^* \rangle_i \leq n_0 \beta \tag{14}$$

This formula is a criterion to identify the belonging to the free surface. Based upon the abovementioned relation, when the temporary particle number density is smaller than a value $n_0\beta$, the free surface condition is assigned to that particle. β is the coefficient for determining the free surface, and here it is 0.92.

3. Results and Discussion

In this paper, the sensitivity analysis of the WC-MPS method for a dam break flow is discussed. To validate the method, experimental data from [14] is adopted and compared with the numerical results. Then, a domain as shown in Fig.1. is considered with a length and height of 3 m and 0.6 m, respectively. The water mass on the left-hand side of the model has 40 cm in both length and height. Two cases are considered to analyze the sensitivity of the WC-MPS for the dam break flow on the dry surface. In the first case, the Courant number is constant, and the results obtained using different particle sizes are compared at various times. The second case concerns the analysis of the sensitivity to the variable Courant number for the fixed particle size.

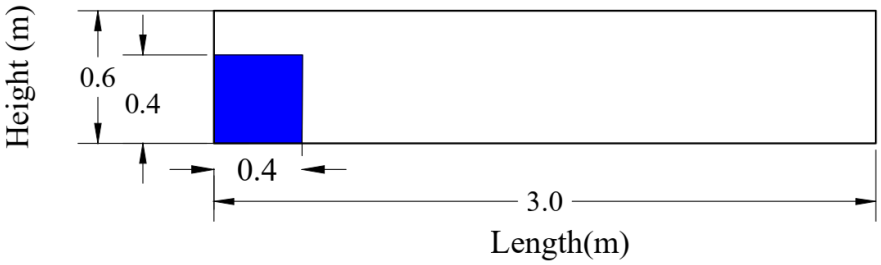

Figure 1. Schematic presentation of dam break model.

3.1. Validation

The aim of this test case is to validate the WC-MPS method with the experimental data. As illustrated in Fig. 2., the initial condition of the channel is set to the experimental model of Ozmen-Cagatay and Kocaman [14]. In a channel with a length of 8.9 m, the water mass is located from -4.65 m to 0 m in the x-direction and 0 to 0.25 m in the y-direction. Additionally, the particle size for the WC-MPS method is set to 0.005 m.

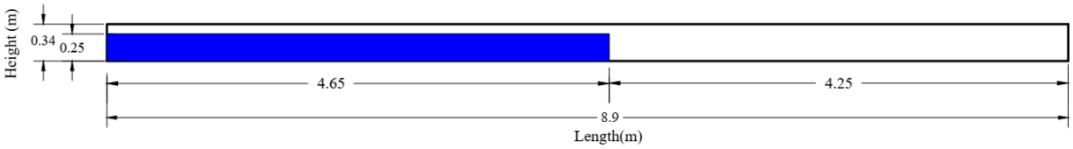

Figure 2. The initial condition of the dam break problem for the validation test case.

The numerical results achieved using the WC-MPS approach are compared with those of experimental measurements [14] in Fig. 3.

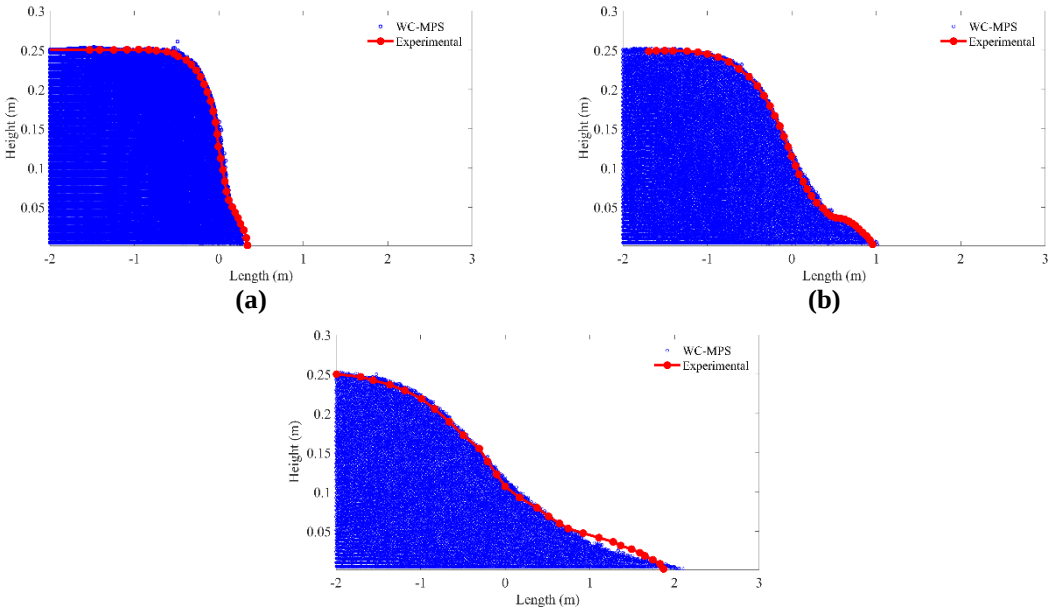

Fig. 3. Comparison between the results of the WC-MPS method (blue particles) with the experimental data (red circle-line) from [14] for the validation dam break test case at *t*= a) 0.18, b) 0.44, and c) 0.80 seconds

As can be observed, the WC-MPS for all computed times gives relatively identical results to experimental data verifying the WC-MPS method.

3.2. Fixed Courant number and variable particle size

The purpose of this case is the sensitivity analysis of the WC-MPS method associated with particle size. Therefore, a fixed Courant number of 0.1 is considered, and the simulation is performed at 0.5, 1, and 1.5 seconds for particle sizes of 0.01, 0.005, and 0.0025 m. In addition, this case is also repeated for Courant numbers 0.5 and 0.9 for more investigation.

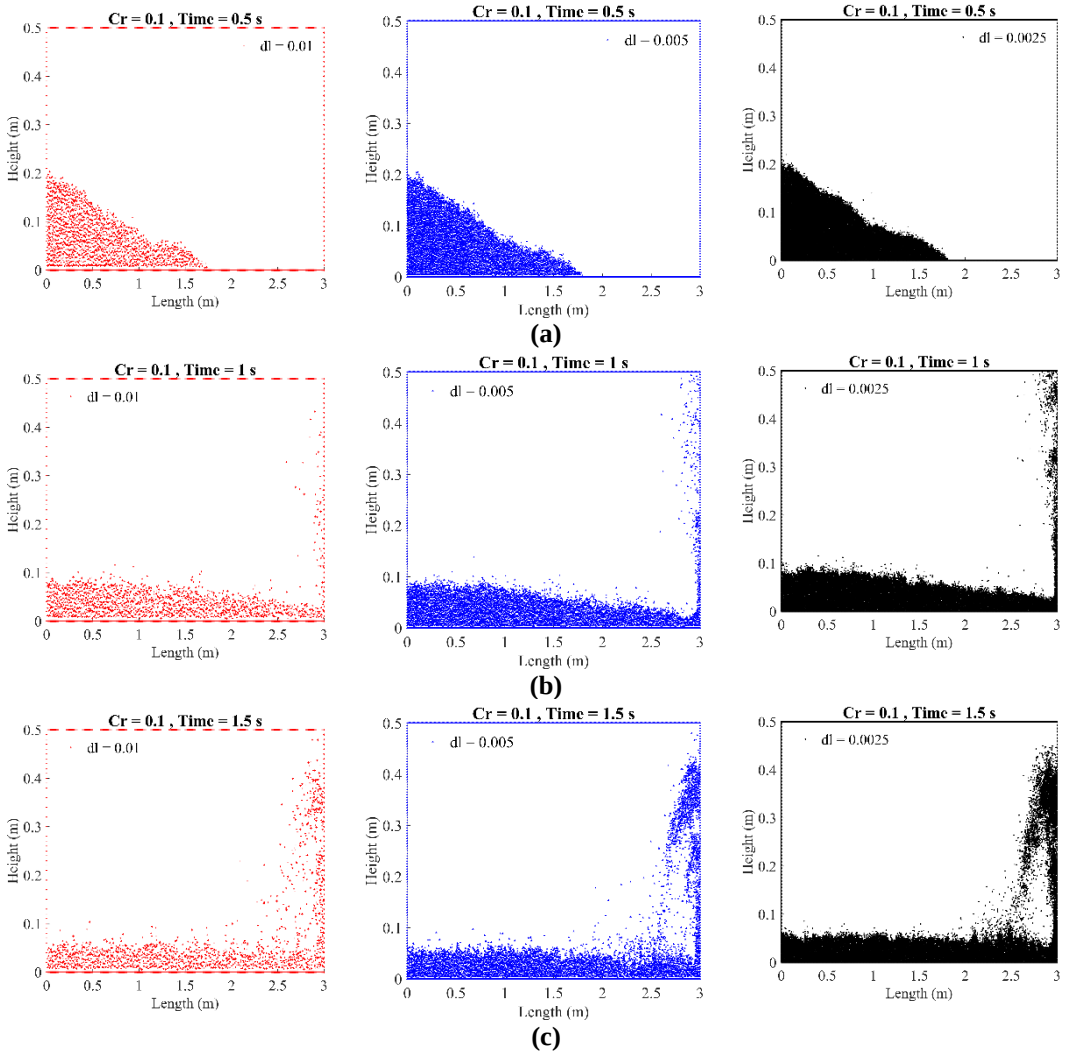

Figure 4. The comparison of the WC-MPS results with fixed Cr=0.1 for different particle sizes at a) 0.5, b) 1, and c) 1.5 seconds

As shown in Fig. 4., at t=0.5 s, the particle size of 0.01 m reaches 1.73 m length whereas dl=0.005 and dl=0.0025 are at 1.79 m and 1.81 m, respectively. After t=1 s, the water collided with the right-hand side wall, reached the top of the computational domain, and moved backward. Based on the observations, it is concluded that the results using dl=0.0025 show the better formation of the cavity and is better concerning the number of returning particles to the water surface.

To compare the accuracy of the WC-MPS method and the VOF solver in more detail, the error norms between the obtained results and the experimental data were calculated using the following equation:

$$\text{Error Norm} = \frac{\sqrt{\sum(dh_i)^2}}{n} \tag{15}$$

where dh_i is the difference of heights of the free-surface flow in the experimental and numerical models at point i, and n shows the number of comparison points. The error norms are calculated for the results shown in Fig. 4. between the experimental data and WC-MPS solution in Table (1). In general, a good level of agreement is obtained between the results.

Table 1. The calculated error norm between the WC-MPS results with fixed Cr=0.1 for particle sizes of dl=0.01m and dl=0.0025 m at 0.5, 1, and 1.5 seconds

Time (s)	Error Norm
0.5	1.4381×10^{-5}
1	1.9624×10^{-5}
1.5	3.4251×10^{-5}

A similar comparison with the Courant number of 0.5 is as follows:

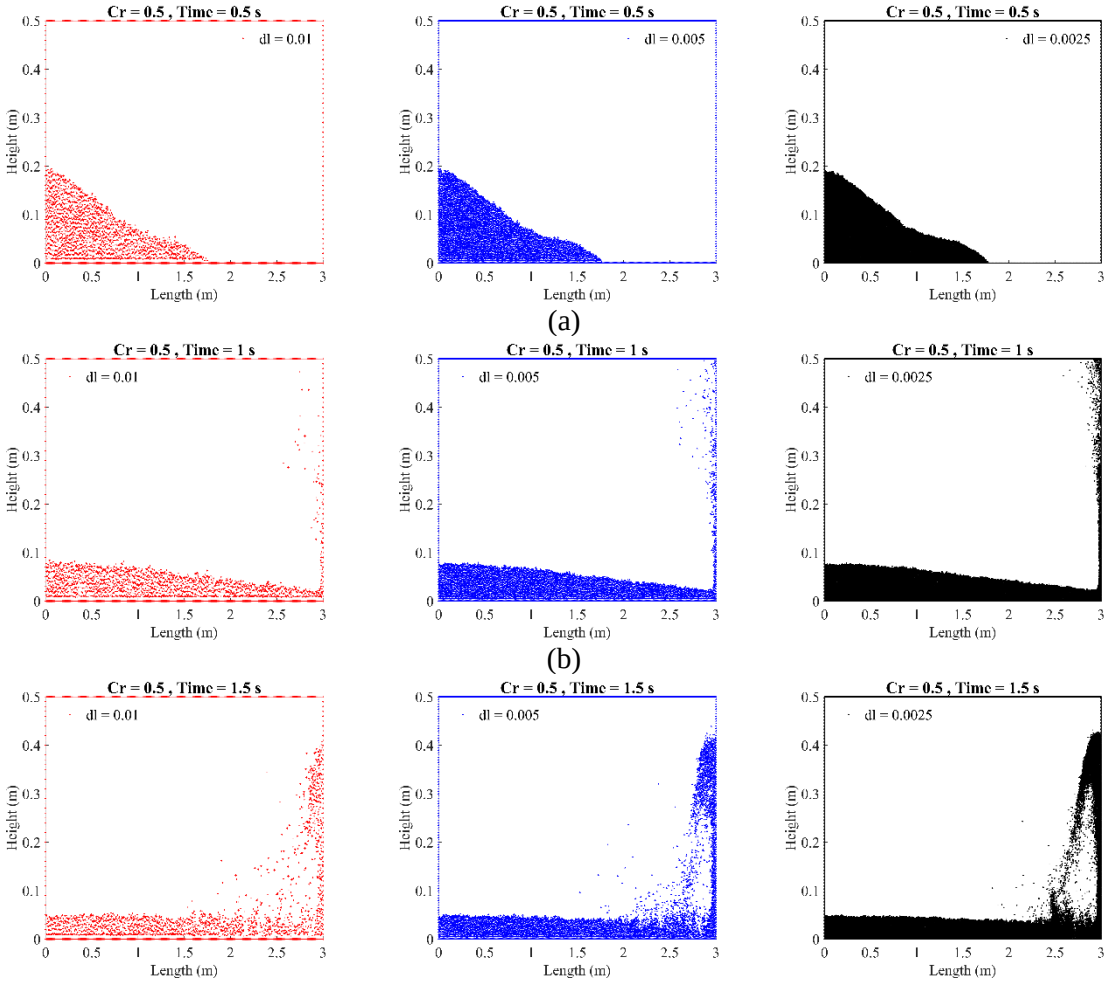

Figure 5. The comparison of the WC-MPS results with fixed *Cr*=0.5 for different particle sizes at a) 0.5, b) 1, and c) 1.5 seconds

Generally, in this case, the Courant number is fixed at 0.5, and a similar condition exists. The only difference is in the values of wavefront movement, which is smaller. For example, at t=0.25 s, the results with dl=0.0025 and dl=0.005 are relatively identical and about one cm more than dl=0.01, while these values are less than the amounts of movement with the Courant number of 0.1. This fact is also actual for the following times. Furthermore, a similar comparison is performed with the Courant number of 0.9 and is depicted in Fig. 6.

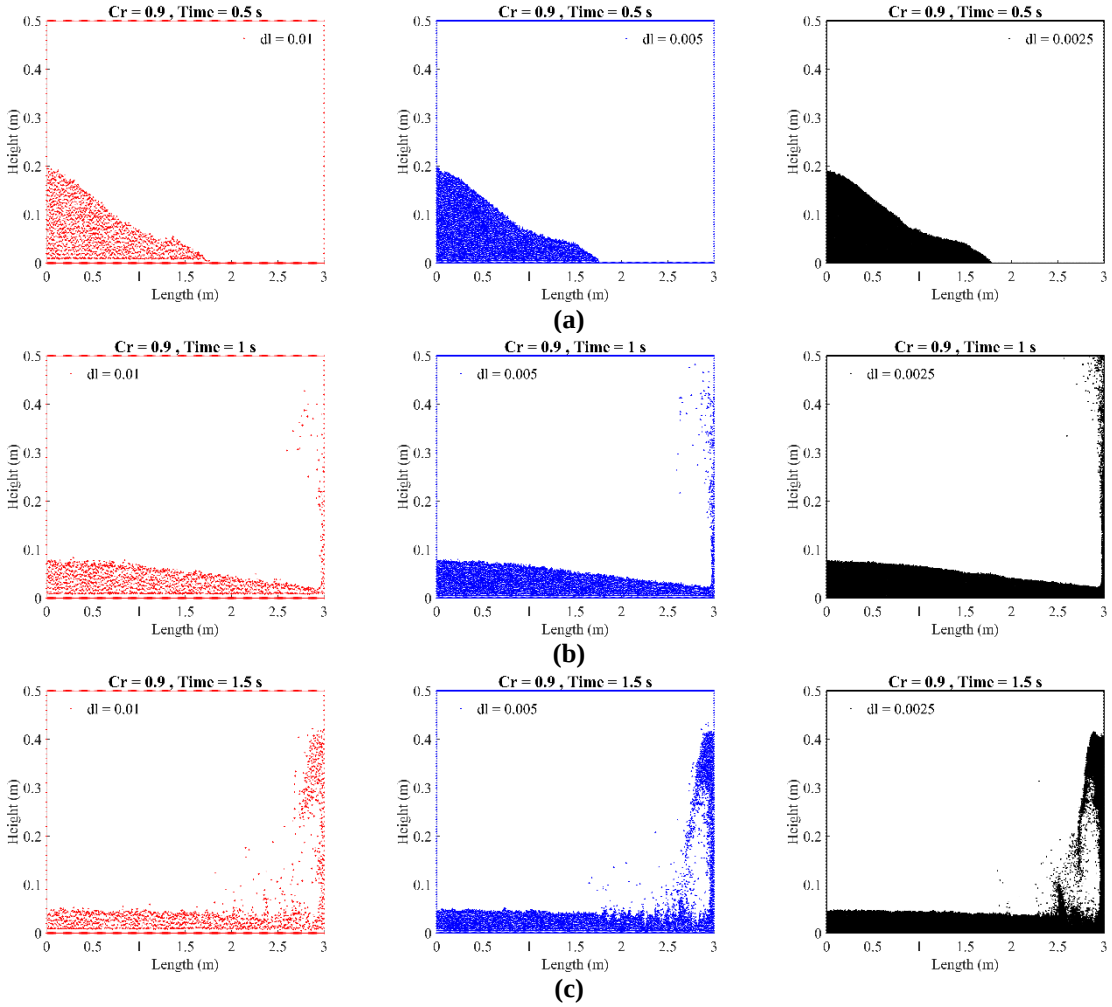

Figure 6. The comparison of the WC-MPS results with fixed *Cr*=0.9 for different particle sizes at a) 0.5, b) 1, and c) 1.5 seconds

There is no significant difference between this condition and the *Cr*=0.5 state. In addition, the quantities of wavefront movements are almost the same. The correlation of particles is higher with smaller particles, and the flow formation is better.

3.3. Fixed particle size and variable Courant number

The objective of this simulation is the investigation the method relative to the Courant number. Therefore, the particle size is considered fixed, and the dam-break model is simulated at *t*=0.5, 1, and 1.5 seconds for Courant numbers of 0.3, 0.5, and 0.7.

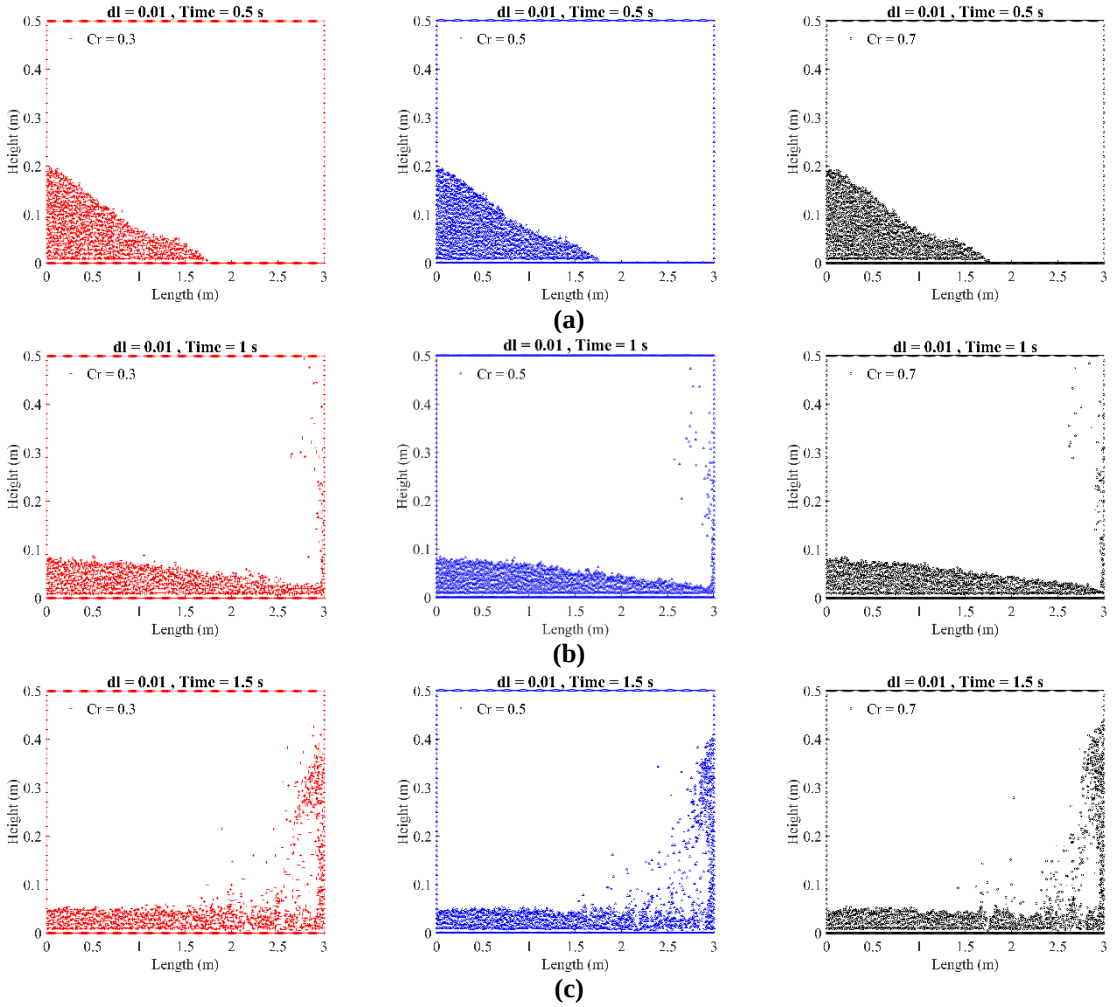

Figure 7. The comparison of the WC-MPS results with fixed *dl*=0.01 m for different Courant numbers at a) 0.5, b) 1, and c) 1.5 seconds

The simulation results using different Courant numbers with fixed *dl*=0.01 m are somewhat identical at *t*=0.25 s. it can be concluded from the results at *t*=1.25 s and *t*=1.5 s that the cavity is formed better, and the value of wavefront movement is higher with *Cr*=0.3. Again, the error norms between the numerical and experimental results are calculated in Table (2).

Table 2. The calculated error norm between the WC-MPS results with fixed dl=0.01 for Courant numbers of Cr=0.3 and Cr=0.7 at 0.5, 1, and 1.5 seconds

Time (s)	Error Norm
0.5	1.1924×10^{-6}
1	1.2683×10^{-6}
1.5	1.5391×10^{-6}

More observation with smaller particle sizes is needed to reach a better conclusion. Therefore, a similar comparison is performed using *dl*=0.005 m and *dl*=0.0025 m, as shown in Fig. 8 and Fig. 9, respectively.

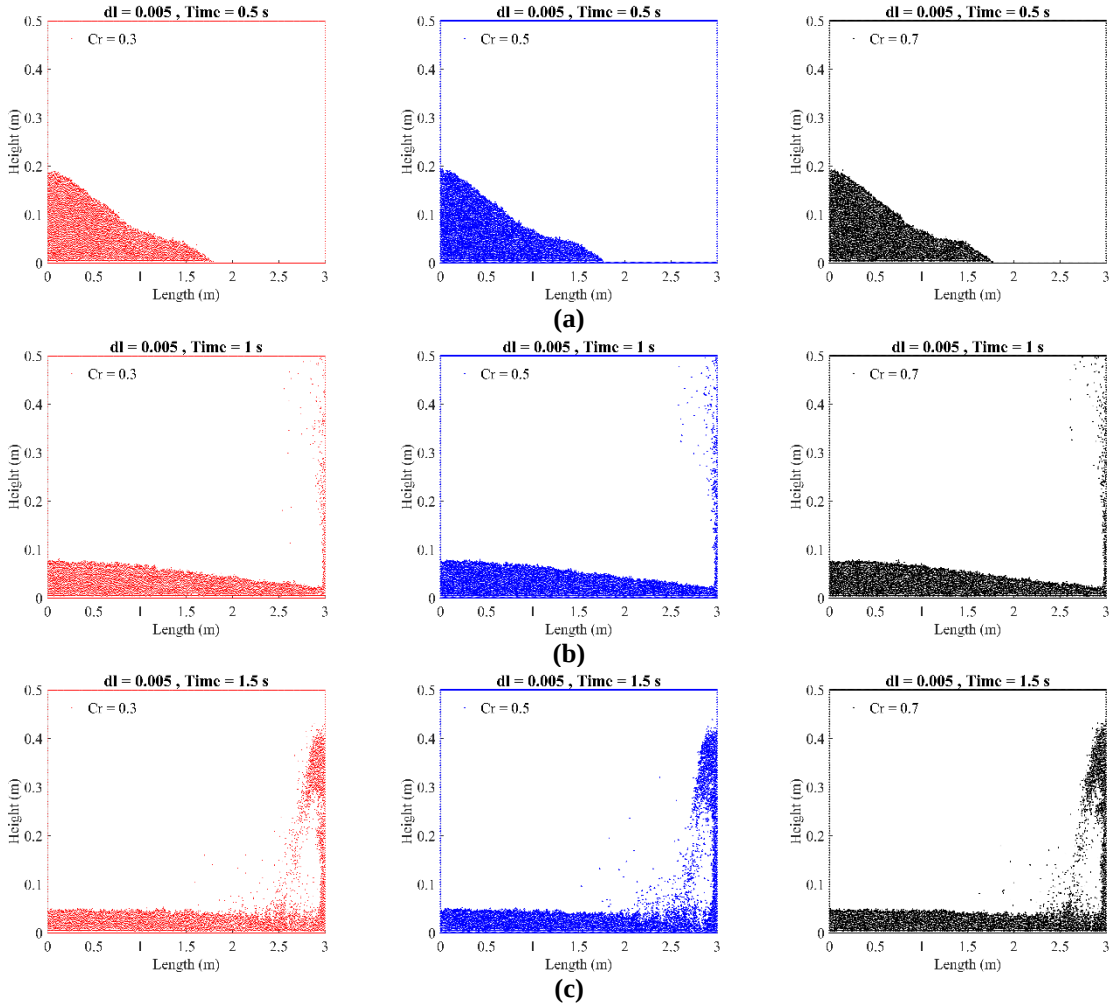

Fig. 8. The comparison of the WC-MPS results with fixed dl=0.005 m for different Courant numbers at a) 0.5, b) 1, and c) 1.5 seconds

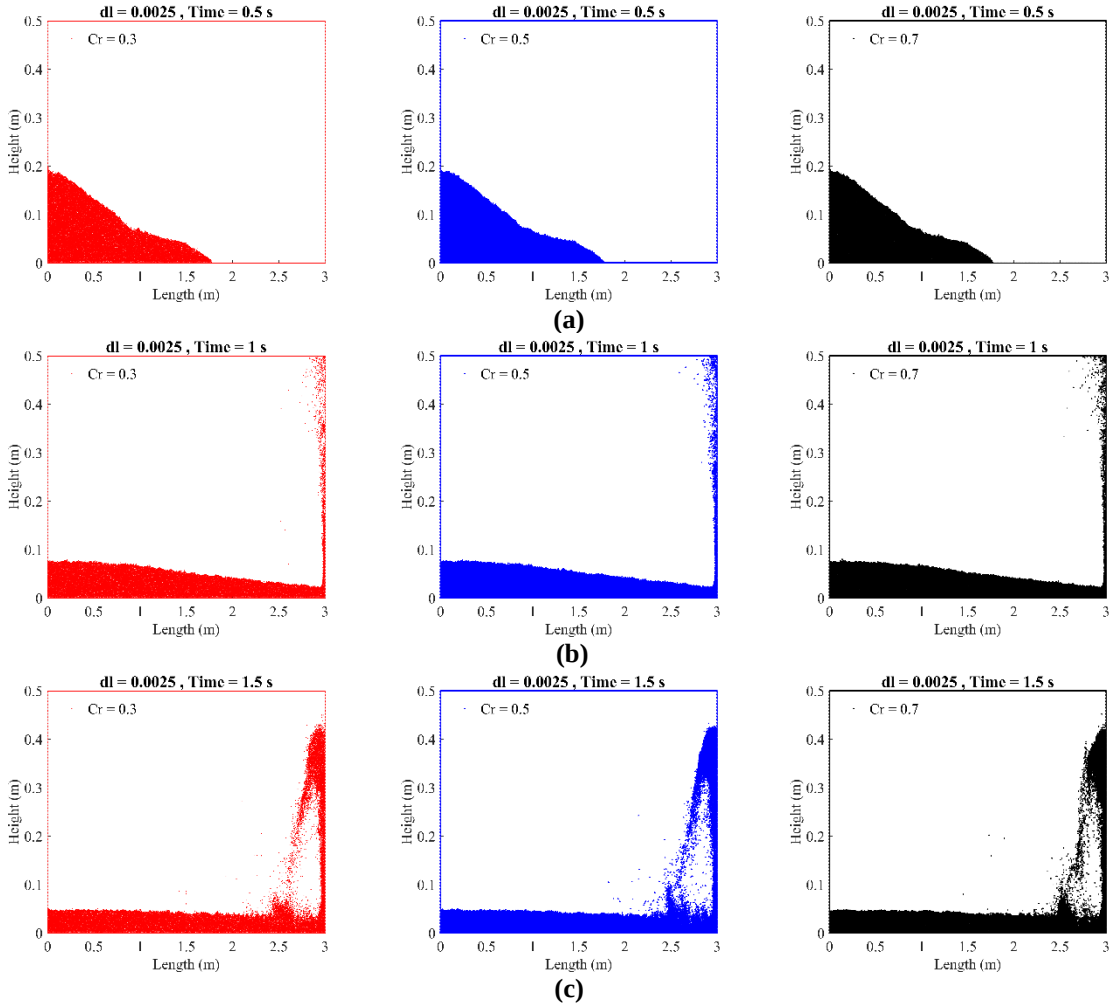

Fig. 9. The comparison of the WC-MPS results with fixed *dl*=0.0025 m for different Courant numbers at a) 0.5, b) 1, and c) 1.5 seconds

As can be seen, the formation of the cavity and the complete form of the flow are better with smaller Courant numbers, and the wavefront movement is more significant at the same time. Furthermore, the effect of particle size is evident in the above Figures, as mentioned in case 1.

4. Conclusions

The ability of the Lagrangian methods such as MPS and SPH to modelling turbulent flows with large deformations has increased the popularity of these methods against Eulerian mesh-based methods. In this study, the dam-break flow on a dry bed was modeled using the WC-MPS method, and its sensitivity to particle size and courant number was investigated in two cases. First, the Courant number was assumed to be constant, and the results were compared in different particle sizes. For this purpose, The Courant number was fixed at 0.1, and the solution obtained with particle sizes of 0.01, 0.005, and 0.0025 m were compared at times of 0.5, 1, and 1.5 seconds. Additionally, the error norms between the numerical and experimental results were calculated. For further study, this process was repeated using values 0.5 and 0.9 for the Courant number. It was observed that in a fixed Courant number, the smaller the particle size, the higher

the wavefront movement, which is closer to reality. Furthermore, the correlation of particles was higher at smaller particle sizes, and the general formation of the flow was better. In the second case, the sensitivity concerning the Courant number was examined by fixing the particle size. In a similar process, the particle size was fixed at 0.01 m, and the results of using the values 0.3, 0.5, and 0.7 for the Courant number were compared at similar times and again the error norms were calculated. For more certainty, the results were shown by fixing the particle size at 0.005 and 0.0025 m. In this case, it was also observed that the smaller the Courant number in fixed particle size, the better the overall flow form and cavity formation. In addition, the wavefront movement increases with decreasing Courant number. From all the observations, it can be concluded that the smaller the particles and the smaller the Courant number, the better and more realistic the results. This difference continues until reaching a balance. For example, in the first case, there was not much difference between the results of $Cr = 0.9$ and $Cr = 0.5$. In the second case, $dl = 0.005$ and $dl = 0.0025$ were not significantly different. However, it is important to note that the computational cost significantly increases by decreasing the Courant numbers and particle size, so the sensitivity analysis should be performed on numerical methods.

References

1. Chanson H, (2009). Application of the method of characteristics to the dam break wave problem. Journal of Hydraulic Research, pp: 47(1): 41-49.
2. Jánosi IM, Jan D, Gábor Szabó K, Tél T, (2004). Turbulent drag reduction in dam-break flows. Experiments in Fluids, pp: 37(2): 219-229.
3. Liao C. B, Wu M. S, Liang S. J, (2007). Numerical simulation of a dam break for an actual river terrain environment. Hydrological Processes: An International Journal, pp: 21(4): 447-460.
4. Wu W, Wang S. S, (2007). One-dimensional modeling of dam-break flow over movable beds. Journal of hydraulic engineering, pp: 133(1): 48-58.
5. Spinewine B., Two-layer flow behaviour and the effects of granular dilatancy in dam-break induced sheet-flow. PhD Thesis, Univerisité de Louvain, Belgium, 2005.
6. Zech Y, Soares-Frazão S, Spinewine B, Le Grelle N, (2008). Dam-break induced sediment movement: Experimental approaches and numerical modelling. Journal of Hydraulic research, pp: 46(2): 176-190.
7. Xia J, Lin B, Falconer L. A, Wang G, (2010). Modelling dam-break flows over mobile beds using a 2D coupled approach. Advances in Water Resources, pp: 33(2): 171-183.
8. Fraccarollo L, Toro E.F, (1995). Experimental and numerical assessment of the shallow water model for two-dimensional dam-break type problems. Journal of hydraulic research, pp: 33(6): 843-864.
9. Aleixo R, Soares-Frazão S, Zech Y, (2011). Velocity-field measurements in a dam-break flow using a PTV Voronoï imaging technique. Experiments in fluids, pp: 50(6): 1633-1649.
10. Lobovský L, Botia-Vera E, Castellana F, Mas-Soler J, Souto-Iglesias A, (2014). Experimental investigation of dynamic pressure loads during dam break. Journal of Fluids and Structures, pp: 48: 407-434.
11. LaRocque L.A, Imran J, Chaudhry M.H, (2013). Experimental and numerical investigations of two-dimensional dam-break flows. Journal of Hydraulic Engineering, pp: 139(6): 569-579.
12. Ritter A, (1892). Die fortpflanzung der wasserwellen. Zeitschrift des Vereines Deutscher Ingenieure, pp: 36(33): 947-954.

13. Deng X, Liu H, Lu S, (2018). Analytical study of dam-break wave tip region. J. Hydraul. Eng, pp: 144(5): 04018015.
14. Ozmen-Cagatay H, Kocaman S, (2011). Dam-break flow in the presence of obstacle: experiment and CFD simulation. Engineering applications of computational fluid mechanics, pp: 5(4): 541-552.
15. Harlow F.H, (1964). The particle-in-cell computing method for fluid dynamics. Methods Comput. Phys., pp: 3: 319-343.
16. Hirt C.W, Nichols B.D, (1981). Volume of fluid (VOF) method for the dynamics of free boundaries. Journal of computational physics, pp: 39(1): 201-225.
17. Liu J, Koshizuka S, Oka Y, (2005). A hybrid particle-mesh method for viscous, incompressible, multiphase flows. Journal of Computational Physics, pp: 202(1): 65-93.
18. Koshizuka S, Nobe A, Oka Y, (1998). Numerical analysis of breaking waves using the moving particle semi-implicit method. International journal for numerical methods in fluids, pp: 26(7): 751-769.
19. Gotoh H, Sakai T, (2006). Key issues in the particle method for computation of wave breaking. Coastal Engineering, pp: 53(2-3): 171-179.
20. Liu G.R., Liu M.B., Smoothed particle hydrodynamics: a meshfree particle method., World scientific, 2003.
21. Mohtashami A, Hashemi Monfared S.A, Azizyan Gh, Akbarpour A, (2021). Estimation of Parameters in Groundwater Modeling by Particle Filter linked to the meshless local Petrov-Galerkin Numerical Method, Journal of Hydraulic Structures, pp: 7(1): 16-37.
22. Mohtashami A, Hashemi Monfared S.A, Azizyan Gh, Akbarpour A, (2021). Numerical simulation of groundwater in an unconfined aquifer with a novel hybrid model (case study: Birjand Aquifer, Iran), Journal of Hydroinformatics, pp: 24(1): 160-178.
23. Gingold R.A, Monaghan J.J, (1977). Smoothed particle hydrodynamics: theory and application to non-spherical stars. Monthly notices of the royal astronomical society, pp: 181(3): 375-389.
24. Lucy L.B, (1977). A numerical approach to the testing of the fission hypothesis. The astronomical journal, pp: 82: 1013-1024.
25. Monaghan J.J, (1994). Simulating free surface flows with SPH. Journal of computational physics, pp: 110(2): 399-406.
26. Moussa B.B, Lanson N, Vila J, (1999). Convergence of meshless methods for conservation laws applications to Euler equations, in Hyperbolic Problems: Theory, Numerics, Applications. pp: 31-40.
27. Ferrari A, Dumbser M, Toro E.F, Armanini A, (2009). A new 3D parallel SPH scheme for free surface flows. Computers & Fluids, pp: 38(6): 1203-1217.
28. Ferrari A, (2010). SPH simulation of free surface flow over a sharp-crested weir. Advances in Water Resources, pp: 33(3):270-276.
29. Hui Pu J, Shao S, Huang Y, (2013). Evaluations of SWEs and SPH numerical modelling techniques for dam break flows. Engineering Applications of Computational Fluid Mechanics, pp: 7(4): 544-563.
30. Yang Q, Jones V, McCue L, (2012). Free-surface flow interactions with deformable structures using an SPH–FEM model. Ocean engineering, pp: 55: 136-147.
31. Koshizuka S, Oka Y, (1996). Moving-particle semi-implicit method for fragmentation of incompressible fluid. Nuclear science and engineering, pp: 123(3): 421-434.

32. Lee E.S, Moulinec C, Xu R, Violeau D, Laurence D, Stansby P, (2008). Comparisons of weakly compressible and truly incompressible algorithms for the SPH mesh free particle method. Journal of computational Physics, pp: 227(18): 8417-8436.
33. Shakibaeinia A, Jin Y.C, (2010). A weakly compressible MPS method for modeling of open-boundary free-surface flow. International journal for numerical methods in fluids, pp: 63(10): 1208-1232.
34. Khayyer A, Gotoh H, (2010). On particle-based simulation of a dam break over a wet bed. Journal of Hydraulic Research, pp: 48(2): 238-249.
35. Shakibaeinia, A., Jin, Y., (2009). Lagrangian modeling of flow over spillways using moving particle semi-implicit method. in Proceeding of 33rd IAHR Congress: Water Engineering for a Sustainable Environment, pp: 1809-1816.
36. Khayyer A, Gotoh H, (2012). A 3D higher order Laplacian model for enhancement and stabilization of pressure calculation in 3D MPS-based simulations. Applied Ocean Research, pp: 37: 120-126.
37. Xu T, Jin Y.C, (2016). Improvements for accuracy and stability in a weakly-compressible particle method. Computers & Fluids, pp: 137: 1-14.
38. Tsuruta N, Khayyer A, Gotoh H, (2013). A short note on dynamic stabilization of moving particle semi-implicit method. Computers & Fluids, pp: 82: 158-164.
39. Khayyer A, Gotoh H, Shimizu Y, (2017). Comparative study on accuracy and conservation properties of two particle regularization schemes and proposal of an optimized particle shifting scheme in ISPH context. Journal of Computational Physics, pp: 332: 236-256.
40. Fu L, Jin Y.C, (2014). Simulating velocity distribution of dam breaks with the particle method. Journal of Hydraulic Engineering, pp: 140(10): 04014048.
41. Xu T, Jin Y.C, (2019). Modeling impact pressure on the surface of porous structure by macroscopic mesh-free method. Ocean Engineering, pp: 182: 1-13.
42. Shakibaeinia A, Jin Y.C, (2011). A mesh-free particle model for simulation of mobile-bed dam break. Advances in Water Resources, pp: 34(6): 794-807.
43. Dalrymple R.A, Rogers B, (2006). Numerical modeling of water waves with the SPH method. Coastal engineering, pp: 53(2-3): 141-147.
44. Courant R, Friedrichs K, Lewy H, (1967). On the partial difference equations of mathematical physics. IBM journal of Research and Development, pp: 11(2): 215-234.

© 2022 by the authors. Licensee SCU, Ahvaz, Iran. This article is an open access article distributed under the terms and conditions of the Creative Commons Attribution 4.0 International (CC BY 4.0 license) (http://creativecommons.org/licenses/by/4.0/).